BRAIN
A JOURNAL OF NEUROLOGY

The neurophysiological correlates of motor tics following focal striatal disinhibition

Kevin W. McCairn,[1,3,]* Maya Bronfeld,[1,]* Katya Belelovsky[1] and Izhar Bar-Gad[1,2]

1 The Leslie & Suzan Gonda Brain Research Center, Bar-Ilan University, Israel
2 The Mina & Everard Goodman Faculty of Life Sciences, Bar-Ilan University, Israel
3 The Open University, Milton Keynes, Dept of Biological Sciences, MK7 66A, UK

*These authors contributed equally to this work.

Correspondence to: Kevin W. McCairn,
The Leslie & Suzan Gonda Brain Research Center,
Bar-Ilan University,
Israel
E-mail: kevin.mccairn@yahoo.com

The cortico-basal ganglia pathway is involved in normal motor control and implicated in multiple movement disorders. Brief repetitive muscle contractions known as motor tics are a common symptom in several basal ganglia related motor disorders. We used focal micro-injections of the GABA-A antagonist bicuculline to the sensorimotor putamen of behaving primates to induce stereotyped tics similar to those observed in human disorders. This focal disruption of GABA transmission in the putamen led to motor tics confined to a single or a few muscles. The temporal and structural properties of the tics were identified using electromyogram and frame-by-frame analysis of multi-camera video recordings. During experimental sessions the tics would wax and wane, but their size and shape remained highly stereotyped within the session. Neuronal spiking activity and local field potentials were recorded simultaneously from multiple locations along the cortico-basal ganglia pathway: motor cortex, putamen and globus pallidus external and internal segments. The local field potentials displayed stereotyped tic-related voltage transients lasting several hundred milliseconds. These 'local field potential spikes', which appeared throughout the cortico-basal ganglia pathway, were consistently observed in close temporal association to the motor tics. During tic expression, neuronal activity was altered in most of the recorded neurons in a temporally focal manner, displaying phasic firing rate modulations time locked to the tics. Consistent with theoretical models of tic generation, transient inhibition of the basal ganglia output nucleus prior to and during tic expression was observed. The phasic reduction of basal ganglia output was correlated with a disinhibition of cortical activity, manifesting as short bursts of activity in motor cortex. The results demonstrate that the basal ganglia provide a finely timed disinhibition in the output nuclei of the basal ganglia. However, a large fraction of the neurons were simultaneously inhibited during tics, although tics were only manifested in a small confined muscle group. This suggests that rather than representing a specific action within the basal ganglia itself, these nuclei provide a temporally exact but spatially distributed release signal. The tics induced by striatal disinhibition bear a striking resemblance to motor tics recognized in human pathologies associated with basal ganglia dysfunction. The neuronal changes observed during tic formation may provide valuable insights into the underlying mechanism of tic disorders, as well as into basic information processing in the cortico-basal ganglia loop.

Introduction

Sudden, brief, jerk-like movements that interfere with ongoing activity are a symptom observed in a wide range of movement disorders (de la Tourette, 1885; Obeso *et al.*, 1983; Jankovic and Ashizawa, 1995; Zohar *et al.*, 1997; Caviness and Brown, 2004; Defebvre, 2006; Vercueil, 2006). These involuntary movements vary in form, severity and anatomical position depending on the associated underlying pathology. Tourette syndrome patients manifest such involuntary movements ranging from simple motor tics that involve only one or a few muscle groups, to complex motor or vocal tics that involve sequential activation of several muscle groups (The Tourette Syndrome Classification Study Group, 1993). Human tic disorders have been associated with abnormalities in the action control pathways of the cortico-basal ganglia loop (Albin *et al.*, 1989; Singer and Minzer, 2003; Kalanithi *et al.*, 2005).

The basal ganglia are a group of subcortical interconnected nuclei, receiving information from most of the cortex and sending information back to it via the thalamus. Information is transmitted throughout the loop via partially overlapping parallel pathways conveying motor, associative and limbic signals (Alexander *et al.*, 1986; Percheron and Filion, 1991). The input nuclei of the basal ganglia, which receive excitatory projections from the cortex and the thalamus are the striatum (subdivided into the caudate nucleus and putamen) and the subthalamic nucleus (STN). The intrinsic nuclei are the inhibitory globus pallidus external segment (GPe) and the modulatory dopaminergic substantia nigra pars compacta. The output nuclei of the system, the globus pallidus internal segment (GPi) and the substantia nigra pars reticulata, send their inhibitory output to the cortex via the thalamus (for a review see Parent and Hazrati, 1995; Gerfen and Wilson, 1996; Bolam *et al.*, 2000).

Early studies found that disruption of normal information transmission in different parts of the basal ganglia of rodents and primates, either by microinjections of pharmacological agents or lesions, could induce different hyperkinetic states. The specific nature of the hyperkinetic movements was dependent on the site of intervention: microinjections of GABA antagonists into GPe induced choreic movements (Crossman *et al.*, 1988) or complex hyperkinetic behaviours (Francois *et al.*, 2004; Grabli *et al.*, 2004), lesion or inactivation of the STN induced hemiballism (Crossman *et al.*, 1984), and microinjections of GABA antagonists into the sensorimotor striatum induced myclonic motor tics (Marsden *et al.*, 1975; Tarsy *et al.*, 1978; Crossman *et al.*, 1988; Worbe *et al.*, 2008).

Early models used these findings to construct a hypothesis of basal ganglia dysfunction leading to hyperkinetic disorders in the context of the 'box and arrow' model (Albin *et al.*, 1989; DeLong, 1990). This model assumes that the basal ganglia influence behaviour by changing (reducing or facilitating) overall cortical excitability through the interplay of two opposing pathways. The 'direct' (striatum → GPi) pathway has an excitatory effect on the cortex whereas the 'indirect' (striatum → GPe → STN → GPi) pathway has an inhibitory net effect on the cortex. According to this model, hyperkinetic disorders are a result of increased excitability of the cortex due to a reduction in GPi activity, caused either by a loss of excitatory drive from the STN or by an increase of inhibitory inputs from the GPe and/or striatum (Albin *et al.*, 1989; DeLong and Wichmann, 2007). These models do not differentiate between different hyperkinetic disorders, and do not address the specific pathophysiology underlying motor tics.

Addressing the specific temporal and spatial properties of both normal behaviour and abnormal symptoms required a more detailed model. Network level models drew on the basic concepts of the box and arrow model, and extended it to incorporate interactions within the nuclei to view the basal ganglia as performing a process of action selection. In these models, the basal ganglia are viewed as initiating or modulating behaviour by choosing one or more actions out of a multitude of actions presented to them by the cortex (Beiser and Houk, 1998; Redgrave *et al.*, 1999; Tepper *et al.*, 2004). Thus, in the normal state, enhanced activity in a small group of striatal neurons leads to a focused inhibition of a group of pallidal neurons. This is accompanied by diffused activation of the rest of the nucleus via opposing signals through the direct and indirect pathways. This activation pattern in the basal ganglia output structure leads to the disinhibition or release of a specific cortical driven behaviour while suppressing all other competing behaviours (Mink, 1996). In the context of basal ganglia related hyperkinetic disorders, these models predict that a dysfunction within the basal ganglia circuit could lead to the impaired inhibition of competing actions (Mink, 2003). Specifically, the expression of tics is viewed as a focal excitatory abnormality in the striatum. This abnormality causes the formation of an erroneously inhibited group of neurons in the GPi that leads to disinhibition of cortical neurons, which release a tic (Mink, 2001; Albin and Mink, 2006).

In this study, we used a model of motor tics in nonhuman primates to explore changes in the activity of single cells and neuronal populations associated with tic expression. We carried out simultaneous recordings of muscle and neural activity in multiple areas along the cortico-basal ganglia loop to explore the tic generating mechanisms.

Methods

Animals

Two Cynomologus monkeys (Monkeys M & I; *Macaca fascicularis*; male; weight: 4–5 kg) were used in this study. The monkeys' health was monitored by a veterinarian, and their fluid consumption, diet and weight were monitored daily. All procedures were in accordance with the National Institutes of Health Guide for the Care and Use of Laboratory Animals (1996) and Bar-Ilan University guidelines for the Use and Care of Laboratory Animals in Research. The experiments were approved and supervised by the Institutional Animal Care and Use Committee (IACUC).

Surgical procedure

The surgical procedures for cranial implantation were conducted under aseptic conditions using gaseous anaesthesia delivered through tracheal intubation (isoflurane 1–3%, nitrous oxide 1% and oxygen) after induction with Ketamine HCl (10 mg/kg) and Domitor

(0.1 mg/kg). Cranial implantation utilized rectangular cilux chambers (27 mm × 27 mm) (Alpha-Omega Engineering, Nazareth, Israel), which were implanted stereotaxically to allow access to the motor cortex and basal ganglia using a coronal approach. The recording chambers were tilted at 40° (monkey M) or 35° (monkey I) in the coronal plane with their centre targeted to the middle of the globus pallidus: stereotactic coordinates A13, L8 and H3 (Szabo and Cowan, 1984). The chambers were fixed into place using titanium bone screws and methyl-methacrylate cement. In addition, a head-holder connector and an electroencephalogram (EEG) screw (Crist Instrument, Hagerstown, MD, USA) were attached to the skull. Prophylactic antibiotics and analgesics were administered post-surgically.

Experimental setup

Animals were trained to sit in a primate chair and were allowed to complete a simple sensorimotor task for delivery of a liquid reward. The performance of the task was not necessary for completion of the experiment and was introduced to reduce excessive spontaneous movement during recording sessions. Spontaneous behaviours and task execution were observed and recorded during each experimental session using a multi-channel video system (GV-800, Geovision, Taiwan) and digital feedback from the behavioural system. The system was designed to visualize behavioural sequences from four different locations: face, upper limbs, lower limbs and the behavioural task. Digital images from each of the separate cameras were captured at 25 frames s^{-1} and stored on a hard disk for offline analysis. In monkey I, in addition to the video acquisition, electromyogram (EMG) signals were sampled from four muscles: biceps, triceps and zygomaticus major and ventral orbicularis oris. EMG wires were constructed from 60 μm Teflon coated silver wire (A-M systems, WA, USA). The EMG wires were percutaneous and inserted immediately prior to each experimental session using a 30-gauge hypodermic needle. EMG signals were sampled at 1.25 kHz and band pass filtered (5–450 Hz, 4 pole Butterworth filter). The EMG signals were processed offline and the envelope was estimated by rectifying the signal, followed by low pass filtering (10 Hz, 8 pole Butterworth filter). Detection of tics utilized the rectified and filtered EMG signal via a threshold crossing method (3 STD over the steady state mean). Behavioural events were identified using frame-by-frame video analysis and aligned to EMG activity to exclude non-relevant muscular activity.

Electrophysiological recording

Following recovery from surgery each animal underwent microelectrode guided mapping of the striatum, GPe and GPi. In monkey I, primary motor cortex was also mapped. During the mapping and the subsequent recording sessions, the monkey's head was immobilized. Functional areas of the motor cortex were identified using sensory examination and intracortical microstimulation (biphasic 5–20 μA, 20 pulses at 300 Hz). The striatum and globus pallidus were identified by their characteristic neuronal activity and their relation to known anatomical boundaries. Mapping was compared with a standard stereotaxic atlas (Szabo and Cowan, 1984; Martin and Bowden, 2000).

The preliminary mapping process was followed by the experimental sessions. During each experimental session, up to 11 glass-coated tungsten microelectrodes (impedance 250–750 kΩ at 1 kHz) and an injectrode were introduced using two separate manipulating towers that could move each electrode and the injectrode independently with 2 μm resolution (DMT and EPS, Alpha-Omega Engineering) (Supplementary Fig. 1). Extracellular activity was filtered by a wide band pass filter (5 Hz to 8 kHz; 4 pole Butterworth filter), amplified by 2000 (MCP-Plus, Alpha Omega Engineering) and continuously sampled at 40 kHz (AlphaMap, Alpha-Omega Engineering).

Micro-injections

The injectrode was comprised of a 28 gauge stainless steel cannula with a straight tip which was partially encapsulated inside a piercing cannula (25 gauge outer diameter stainless steel cannula with a beveled tip) and a 50 μm Narylene coated microelectrode (Nano-Biosensors, Nazareth, Israel) which was inserted and fixed inside the injection cannula, extending 0.5 mm beyond its tip. Recordings through this electrode were used to determine the depth of injection site within the striatum during each recording session (a detailed description of the recording and injection setup appears in Supplementary 1).

The injection cannula was connected via a Delrin manifold to a 10 μl syringe (Hamilton, Reno, NV, USA), and filled with the injected substance. We used bicuculline (Sigma-Aldrich, Israel) dissolved in physiological saline at a concentration of 15 μg/μl (29.5 mmol/l). The tip of the injection cannula was positioned at the chosen site prior to the beginning of the recording and was left in place during the entire experimental session. Once a sufficient number of separable neurons had been identified on the electrodes and were stable for a minimum of 3 min, bicuculline (2.5–5 μl) was injected at a rate of ~2 μl/min. Previous studies demonstrated that bicuculline injected using similar parameters spread in an ellipsoid with an approximate radius of 1.5 mm around the injection site (Yoshida et al., 1991). Control micro-injections of saline were administered using equivalent amounts and rates at some striatal sites. Additional control bicuculline microinjections were made into the GPe, which is the adjacent nucleus to the striatum.

Off-line analysis of neuronal activity

The wide band recorded extracellular data was split into high- (neuronal spiking activity) and low-frequency activity (LFP) components using high- and low-pass filters, respectively. The action potentials of individual neurons were sorted offline (OfflineSorter V2.8.7, Plexon, Plano, TX, USA). Offline sorting enabled high fidelity in neuronal identification even in neurons that gradually changed their firing properties and spike shapes over time. Neurons were accepted for further analysis if they met the following criteria: (i) the recording was from a location within GPe, GPi or primary motor cortex; (ii) the acquired cells' action potentials were of a consistent distinct shape that could be fully separated with a high degree of certainty from the spike waveforms of other neurons and background noise; (iii) the cells' interspike intervals were confirmed to have a minimum refractory period of 1.5 ms (<0.1% of spikes within the period); and (iv) stable neuronal recording was available for at least 60 s.

Low-frequency activity data was extracted by applying a low pass filter (10 Hz, 8 pole Butterworth filter) to the wide band extracellular signal. Significant voltage transients in the low frequency activity signals, which were termed 'LFP spikes', were detected by a pattern matching method. Initially, the LFP signal was rectified and threshold crossings were detected. LFP spike shapes were reconstructed by finding the largest trough in the LFP signal around threshold crossing and extracting 250 ms of the signal before and after time of trough. After extracting all identified LFP spikes, the mean shape was calculated and the Euclidian distance between this mean shape and each LFP spike was calculated. The mean and standard deviation of the distances were calculated and shapes whose distance was over the 95th

percentile from the mean shape were excluded from further analysis. The mean shape was calculated again using only the valid LFP spike waveforms and mean value and 99% confidence limits of the first 150 ms of this shape were calculated. The beginning of LFP voltage transient was defined as the first time in which the mean shape waveform crossed this confidence limit and all other LFP spike times were corrected accordingly to reflect the start time of the LFP transients (Supplementary Fig. 2).

Data analysis

Following offline sorting of the neuronal data, the spike trains and LFP signals were correlated with behavioural events using MATLAB (V2007B, The Mathworks, Natick, MA, USA) and Neuroexplorer (V4, Nex technologies, Littleton, MA, USA). Behavioural events of interest were identified from frame-by-frame analysis of the digitized video stream. The time stamps derived from the video analysis were then aligned to the processed LFP and EMG data, and used to exclude significant voltage transients that stemmed from spontaneous activity, or were of unknown origin. The time stamps from the LFP that were a result of myoclonic tics were then used to construct peri-event histograms (using 10 ms bins) of the neuronal data. Significance testing of neuronal activity in peri-event histograms was determined by constructing 99% confidence limits based on the mean and standard deviation of the activity within the tail of the histogram (activity at 4–0.5 s prior to the tic). A neuron was considered to have a significant peri-event response if activity crossed the assigned confidence level. All measures in the results section are described as mean $\pm$ SD unless stated otherwise.

Histology

Following completion of the experiment animals were anaesthetized using ketamine 10 mg/kg and stereotactic marking microlesions (DC current 60 µA for 30 s) were made. The lesions were targeted to dorsal white matter tracts at the anatomical plane that was derived from electrophysiological mapping to be consistent with the position of the anterior commisure (AC0). Animals were then deeply anaesthetized using sodium pentobarbital 50 mg/kg and transcardially perfused with 1 l of physiological saline, followed by 1 l of 4% paraformaldehyde. The whole brain was removed and buffered in graded sucrose solution 10%–30% over 7 days. The brain was then frozen at $-25°C$

and cut in the coronal plane using a cryostat (Leica Microsystems, Wetzler, Germany). Each section was digitized using a 10 MPixel digital camera and sections of interest were mounted on to glass slides and Nissl stained. Contours of brain structures were traced using the digitized images and the anterioposterior position of each injection site was plotted relative to the AC–PC axis, taking AC0 as the origin of the system axes.

Software

The MATLAB software used for the data analysis in this article can be found at: http://neurint.ls.biu.ac.il/software/Tics.

Results

A total of 15 bicuculline injections were administered targeting the sensorimotor putamen in two monkeys (eight in monkey M, seven in monkey I, details in Table 1). Microlesion markings shown on the post-mortem anatomical reconstruction confirmed that the microinjections were targeted to the dorsolateral sensorimotor putamen, posterior to the anterior commisure (AC) (Fig. 1A). The distribution of injection sites overlaid on the reconstructed brain (monkey M) confirmed that the injection sites were confined to the targeted locations (Fig. 1B).

Behavioural effect

Analysis of the video data and EMG activity showed that 10/15 (67%) of the bicuculline injections produced major changes in the behavioural state of the animal. The same types of effect were observed for both animals, with simple motor tics contralateral to the injected hemisphere being the predominant response (9/10, 90%), and one session resulting in chorea of the upper limb contralateral to the injection site (Table 1 and Fig. 1B). None of the control bicuculline injections made outside the striatum resulted in the appearance of motor tics, but 9/12 bicuculline GPe microinjections resulted in chorea of the upper or lower limbs. No abnormal movements or behaviours of any kind were observed following control saline injections. Motor tics typically presented as focal,

Table 1 Micro-injections, anatomical and behavioural details

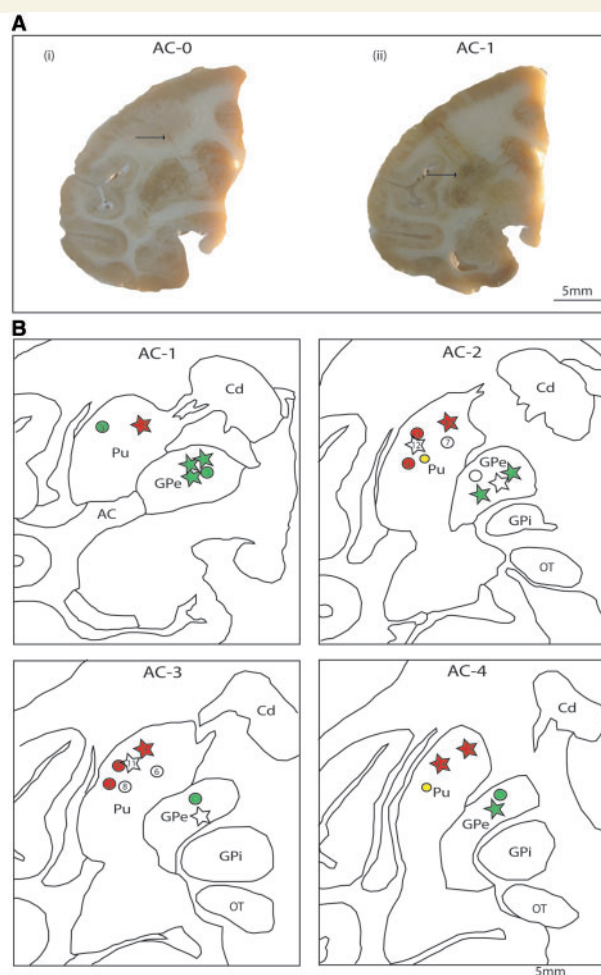| Animal	Inj. No.	AC Plane	Volume (µl)	Onset (min)	Effect	Mean Freq (tics/min)
M	1	−2	5	4	Facial/shoulder tics	27
	2	−3	5	4	Facial tics	21
(*n* = 8)	3	−1	5	6	Chorea	(-)
	4	−2	5	14	Facial tics	14
	5	−3	5	6	Facial tics	18
	6	−3	5	–	No effect	(-)
	7	−2	5	–	No effect	(-)
	8	−3	5	–	No effect	(-)
I	9	−3	5	2	Facial/shoulder tics	63
	10	−2	2.5	5	Facial tics	57
(*n* = 7)	11	−3	5	–	No effect	(-)
	12	−2	5	–	No effect	(-)
	13	−4	2.5	5	Facial tics	29
	14	−4	2.5	3	Facial tics	48
	15	−1	2.5	5	Facial tics	44

Figure 1 Anatomical reconstruction of injection site locations. (**A**) Images of coronal sections of the right hemisphere from monkey M. (i) Pre-euthanasia electrolytic marking lesions (black arrow) targeted to AC0, using reconstructed coordinates derived from electrophysiological mapping. (ii) Gliosis (black arrow) formed by recording electrode trajectories and microinjection site which were targeted to AC-1. (**B**) Outline drawings reconstructed from the coronal sections of the right hemisphere of monkey M. The projected injection sites are derived from electrophysiological mapping and post-mortem reconstruction from each animal overlaid on the same sections. (circles = monkey M, stars = monkey I; red = motor tics; green = chorea; white = no effect; yellow = control injections using saline (*Abbreviations*: AC = anterior commissure; Cd = caudate nucleus; OT = optic tract; Pu = putamen).

sudden, brief jerk-like movements, involving a single body part or muscle group (example in Fig. 2A), and were easily detectable regardless of whether the monkey was at rest or engaged in any other normal behaviour. Tics were stereotypic and repetitive in shape and form, with a single tic event appearing once every several seconds (Table 1). The beginning and end of each single tic event was clearly detectable and separable from the tics preceding or following it. Movements which were classified as choreic were clearly discernable from tics by their longer, smooth, continuous and rotational characteristic. Video segments showing

examples of abnormal movements are shown and discussed in the supplementary material (Supplementary video and Supplementary Fig. 3).

Tics did not interfere with overall normal behaviour, movements and task performance. Following completion of injection delivery, induced tics were detectable within minutes (5.3 ± 3.5 min). The anatomical distribution of the tics was focused primarily within the orofacial region; however, in three cases the shoulder, proximal and distal arm were also affected (Table 1). The tics were clearly detectable from the EMG signal, manifesting as short EMG bursts of one muscle without affecting others (Fig. 2B). Quantification of the properties of each myoclonic event was derived from the rectified and filtered EMG signal (Fig. 2C). The drastic difference in the EMG amplitude during the tic (typically at least 50 times the basal level) enabled the transformation of the signal into a point process of tic events timed at the EMG change initiations. The characteristics of each tic, i.e. duration, amplitude, etc., as defined by the shape of the EMG burst, were highly stereotypic and remained unaltered throughout the recording session (Fig. 2D). The rate of tic events varied across experimental days depending on the injection site (35.7 ± 17.8 tics/min) (Table 1). During each of the sessions, the rate of the tics typically changed gradually; the rate increased following delivery of injection and would wax and wane during the recording process (Fig. 2D). Despite the different tic rates expressed on each experimental day, the overall pattern of tic progression during a day showed similar gradual changes across all days (Fig. 2E). Interspersed within the tic train were sporadic tetanic contractions lasting several seconds that were reflected as short periods of complex EMG activity (Supplementary Fig. 4). The regularity of the tics was assessed using the coefficient of variation (CV), defined as the standard deviation of the inter tic intervals divided by the mean of the inter tic intervals. Coefficient of variation values close to zero represent a completely regular (rhythmic) process, while coefficient of variation values close to 1 represent a Poisson process, in which tics appear irregularly. The coefficient of variation was calculated in bins of 20 s, taken from segments in which tics were well established and there were no tetanic episodes. The mean coefficient of variation for these periods was 0.33 ± 0.12, which reflects a semi-regular process over short periods. However, over longer periods the tic rate would show mild fluctuations (Fig. 2E), which introduced long-term irregularity to the process.

Local field potential activity

Following delivery of bicuculline to the striatum, stereotypic changes in the local field potential 200–400 ms long ('LFP spikes'), would appear in conjunction with the EMG bursts. The LFP spikes appeared simultaneously at all the recorded nodes: cortex, striatum and both segments of the GP (Fig. 3A). The rate of LFP events closely followed that of the EMG tics and would thus vary during experimental sessions and across experimental days. Despite variations in the LFP event rate, the amplitude and duration of each LFP spike within the same session remained stable (Fig. 3B). The shape and amplitude of LFP spikes was variable between different recording sites during a session and between different recording sessions. When comparing
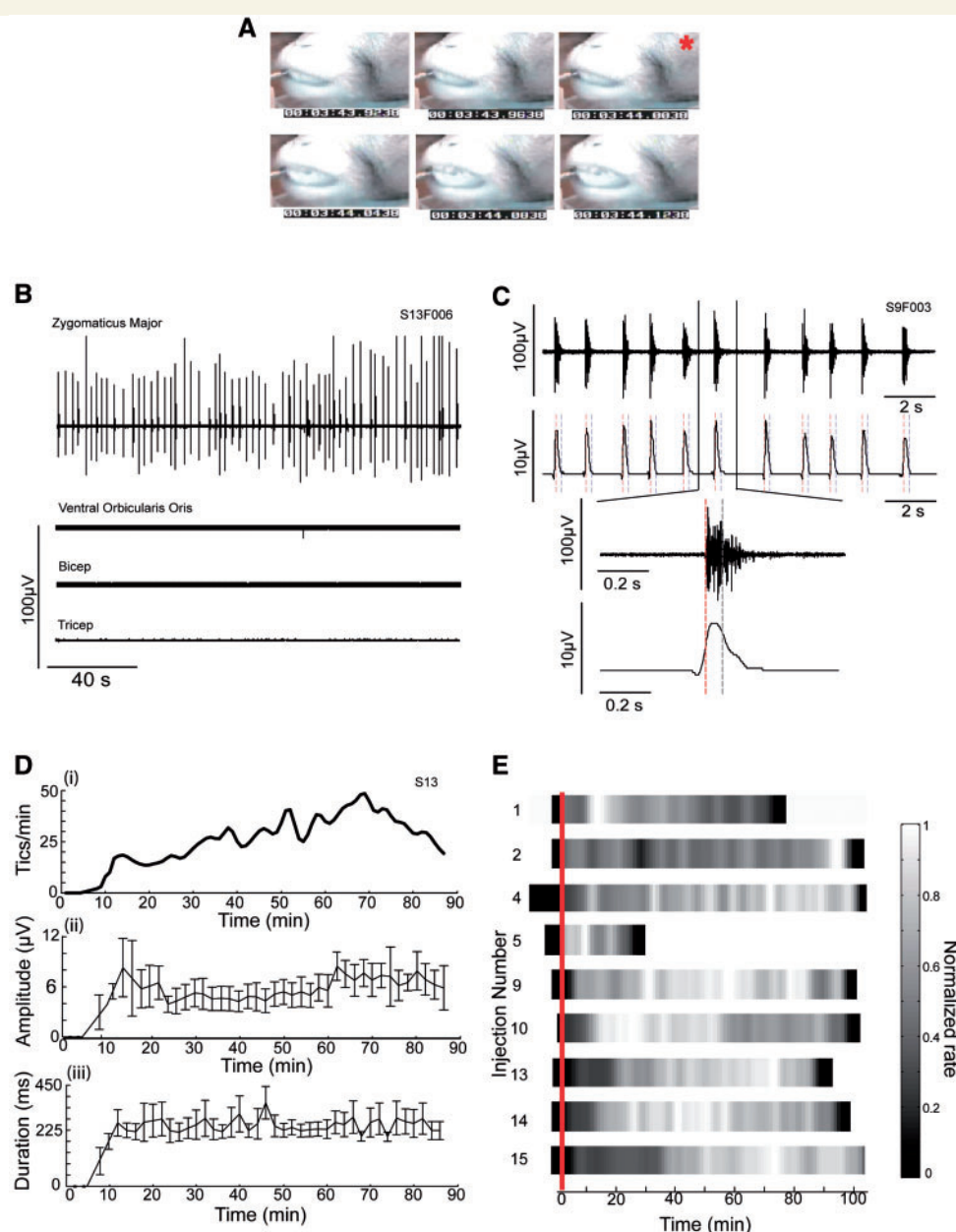
Figure 2 EMG recording and the expression of tics. Video and EMG recordings following injection of bicuclline to the striatum. (**A**) A sequence of six consecutive frames taken from the captured video (25 frames/s) prior to and during an orofacial tic, with activation of the zygomaticus major muscle. The red asterix indicates the tic initiation. (**B**) A simultaneous EMG recording from four different muscles demonstrating the focal nature of the tics. EMG bursts are clearly identifiable in the zygomaticus major muscle, yet no detectable events occur in the other three muscles. (**C**) Expanded example of an EMG trace recorded from the zygomaticus muscle. The figure shows the raw trace (upper) and the same trace following rectification and low pass filtering (lower), and an expanded example of a single event and detection of the tic start time (red dashed line-tic detection from EMG threshold crossing, grey dashed line-tic: detection from video). (**D**) An example of a single experimental session (Monkey I) showing the changes in multiple properties of the tics: (i) rate (ii) amplitude (iii) length. (**E**) The change in tic rate over all recording sessions. The matrix shows the colour coded normalized rate (with the maximum for each session defined as 1) and aligns all the sessions to the onset of the first tic (solid red line). The period before time 0 reflects the latency between the injection and the first tic.

the amplitude of the LFP spikes at each node, it was observed that there was a significant difference in the size of the LFP spikes between the cortex and the deep structures of the basal ganglia, but not between the different nuclei of the basal ganglia (striatum = $157 \pm 21.8\,\mu V$, GPe = $164.2 \pm 25.0\,\mu V$,

GPi = $160.1 \pm 13.8\,\mu V$, primary motor cortex = $464.8 \pm 74.9\,\mu V$, ANOVA $P < 0.01$ *post hoc* pair-wise LSD) (Fig. 3C).

LFP spikes appeared temporally adjacent to the EMG events and video behavioural markers, although sporadic LFP spikes were detected in the absence of an obvious behavioural event.
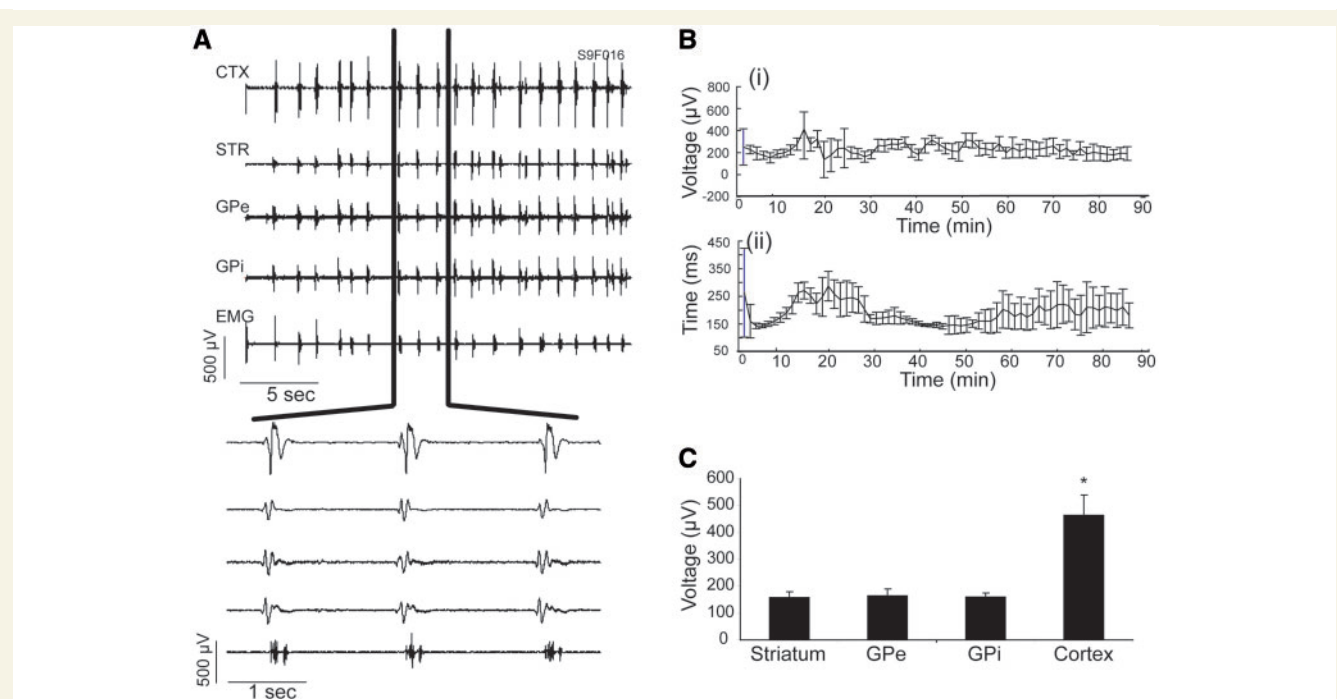
Figure 3 Local field potential activity in the cortico basal ganglia loop. (**A**) Simultaneous recordings of LFP activity in each of the principal nodes of the basal ganglia following delivery of bicuculline and their relation to the EMG. (**B**) Stability of the LFP waveforms during a typical experimental session: (i) amplitude; (ii) length. (**C**) Mean amplitude of LFP spikes in each brain structure across all recording sessions. The LFP spikes' amplitude in the cortex was significantly larger than LFP spikes recorded in the deep structures (*$P < 0.001$).
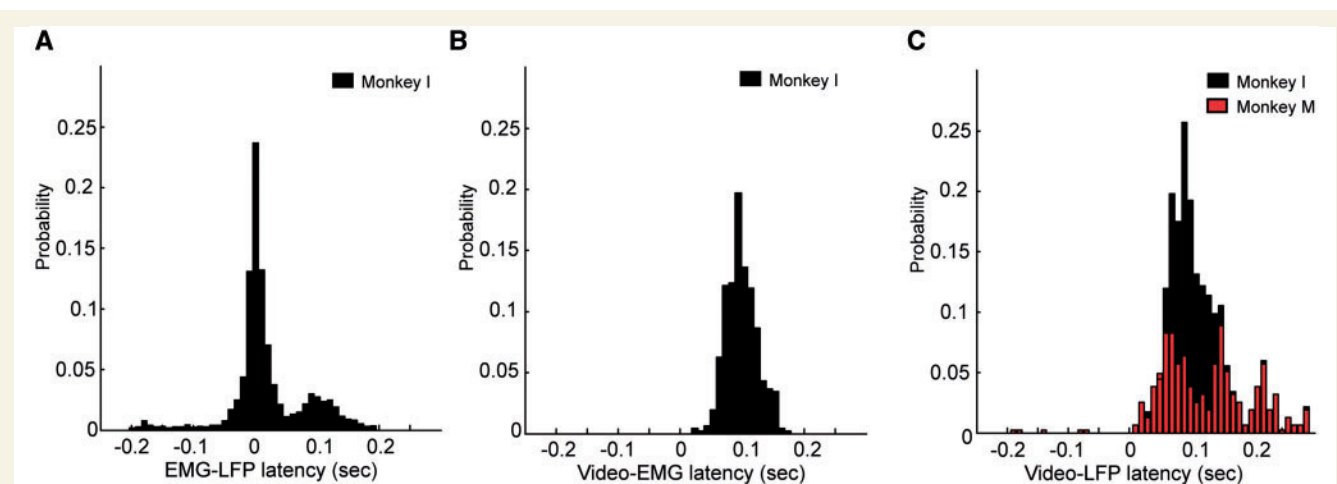

Figure 4 Local field potential activity in relation to behavioural markers. (**A**) Distribution of GPe LFP spike timing in relation to tic identified from EMG activity over all sessions. (**B**) The temporal relation between detection of the tic events derived from samples of the video recording and tic identified from the EMG activity. (**C**) Distribution of the latency between identification of tic events from the video and LFP spikes in both monkeys (histogram is stacked).

LFP spikes appeared predominantly at the same time as the EMG bursts (18.8 ± 60.4 ms) (Fig. 4A). The video identification of tics appeared typically 100 ms after the onset of both the EMG bursts (99 ± 24.7 ms) (Fig. 4B) and the LFP spikes (105.3 ± 49.3 ms) (Fig. 4C). During the tetanic episodes, higher frequency complex waveforms in the LFP, lasting several seconds, were observed

(Supplementary Fig. 4). Due to the strong temporal correlation between LFP spikes and motor tics, we considered the LFP spikes to be a physiological marker of tics, and used them to test the activity of single neurons around tic onset. In all of these analyses, LFP spike times were taken from electrodes located within the GPe.

Single cell activity following bicuculline injection

A total of 130 GPe, 98 GPi and 48 primary motor cortex cells were recorded for this study; of those cells 67 GPe, 77 GPi and 21 primary motor cortex cells were recorded during bicuculline induced tic expression. All primary motor cortex neurons were recorded from areas previously identified as the orofacial region. The neurons of the GPe and GPi were recorded from five coronal planes (AC-2 to AC-6), roughly uniformly distributed throughout the dorso-ventral axis of the nuclei (detailed anatomical reconstruction of the location of all recorded neurons can be found in Supplementary Fig. 5).

Following striatal bicuculline injection and the ensuing expression of motor tics, using the start of the LFP spikes as a physiological marker, peri-tic phasic responses were common in all recorded nodes. In the GPe, 70.3% (47/67) of the cells had a significant peri-event response. Most of the responding GPe cells showed an excitatory phasic response (28/47 cells, 59.5%), but a subset of cells showed inhibitory (4/47 cells, 8.5%) or multiphasic responses (15/47 cells, 32%). The multiphasic responses showed, in similar proportions, an increase followed by a reduction in activity, or an initial small reduction in activity followed by a large increase (8/47 cells, 17% and 7/47 cells, 15%, respectively). We did not observe any topographical organization of the different types of neuronal responses in the GPe (Supplementary Fig. 5). Most of the observed peri-tic related activity began around the time of the LFP spikes (0–70 ms, 25–75% percentiles, respectively) with some significant activity changes as early as 500 ms before the tic (Fig. 5).

A large majority of the recorded GPi cells (64/77 neurons, 83.1%) had a significant peri-tic response. Most of the responding GPi neurons (62%) showed an inhibitory response, either as the only significant response or as a multiphasic response with an initial large inhibitory phase followed by a small increase of activity (20/64 cells in each group). In addition, 26.6% (17/64 cells) of the neurons showed a multiphasic response with a small initial excitatory response, followed by inhibition of activity. Only 14% (9/64 cells) of GPi neurons showed an increase in activity as the only significant response. We did not observe any topographical organization of the different types of neuronal responses in the GPi (Supplementary Fig. 5). Most of the observed peri-tic related activity began around the time of the LFP spikes (0–60 ms, 25–75% percentiles, respectively) with some significant activity changes as early as 200 ms before the tic (Fig. 6).

Following injection and induction of tics, most primary motor cortex (M1) cells (18/21, 86%) transitioned to an abnormal bistable state where they would flip from a state of no activity during the inter tic interval to periods of highly active bursts coinciding with EMG events. The activity within the neuronal burst was typically characterized by a decrementing action potential waveform profile (Fig. 7A). Only a single neuron showed a small decrease of activity followed by a large excitatory phase. Most of the observed peri-tic related activity was centred on the time of the LFP spikes (−35 to 35 ms, 25–75% percentiles, respectively) (Fig. 7).

Discussion

The results presented in this study demonstrate that focal disinhibition of the sensorimotor striatum leads to the formation of repetitive motor tics, confined to single or small groups of muscles predominantly in the orofacial region. The tics vary in rate, but their size and shape remain highly stereotyped. The expression of tics was associated with altered neuronal activity within the cortico-basal ganglia loop. The LFP displayed stereotyped tic-related voltage transients lasting several hundred milliseconds. These LFP spikes were a system-wide phenomenon appearing throughout the cortico-basal ganglia pathway and were highly correlated to the tics. Motor tics were associated with marked phasic changes in the activity of single globus pallidus cells: phasic increases in firing rate were highly prevalent in the GPe, drastic firing rate reductions were observed in almost all GPi cells, and in primary motor cortex, tics were associated with short bursts of increased activity.

The area in which the micro-injections were placed was consistent with striatal areas that receive cortical input from the motor, premotor and somatosensory cortices (Flaherty and Graybiel, 1991; Inase *et al.*, 1996). The primary behavioural effect in this study was orofacial tics caused by activation of the zygomaticus major muscle, resulting in retraction of the upper lip. Previous studies reported that following microinjections of GABA antagonists into striatum, myoclonic tics could be observed in orofacial regions, upper limbs and lower limbs (Tarsy *et al.*, 1978; Crossman *et al.*, 1988; Worbe *et al.*, 2008). In contrast, injections into other areas along the injectrode's path, either more superficial (cortex) or deeper areas (GPe) yielded different behavioural effects (Crossman *et al.*, 1988; Matsumura *et al.*, 1991; Grabli *et al.*, 2004) implying a localized effect of the injection to the striatum. In line with our findings, one study reported orofacial tics as the most prevalent phenomena (Worbe *et al.*, 2008) and all previous studies did not find any correlation between the location of injection sites within the putamen and the appearance of tics in a particular body part. The cause for the focal and stereotyped location of the tics in the current study is unknown. However, the demonstrated over-representation of orofacial areas in the putamen (Miyachi *et al.*, 2006) may account for the higher prevalence of orofacial tics following bicuculline microinjections in our study. Notably, this finding is consistent with the observation that in most human patients suffering from Tourette syndrome, face and neck tics are the first and most common symptom to occur (Kurlan, 2004), possibly suggesting a large representation of these areas in motor-control circuits or their heightened susceptibility to dysfunction.

The periodic nature of the tic events was sometimes interspersed with tetanic episodes in which a burst of frequently occurring tics would appear, usually lasting several seconds. Similar behavioural events have previously been described in this model (McKenzie and Viik, 1975; Tarsy *et al.*, 1978; Crossman *et al.*, 1988; Darbin and Wichmann, 2008; Worbe *et al.*, 2008), but they have not been studied in detail. These events seem to appear irregularly during the course of tic expression following bicuculline micro-injections, and the causes and neural correlates
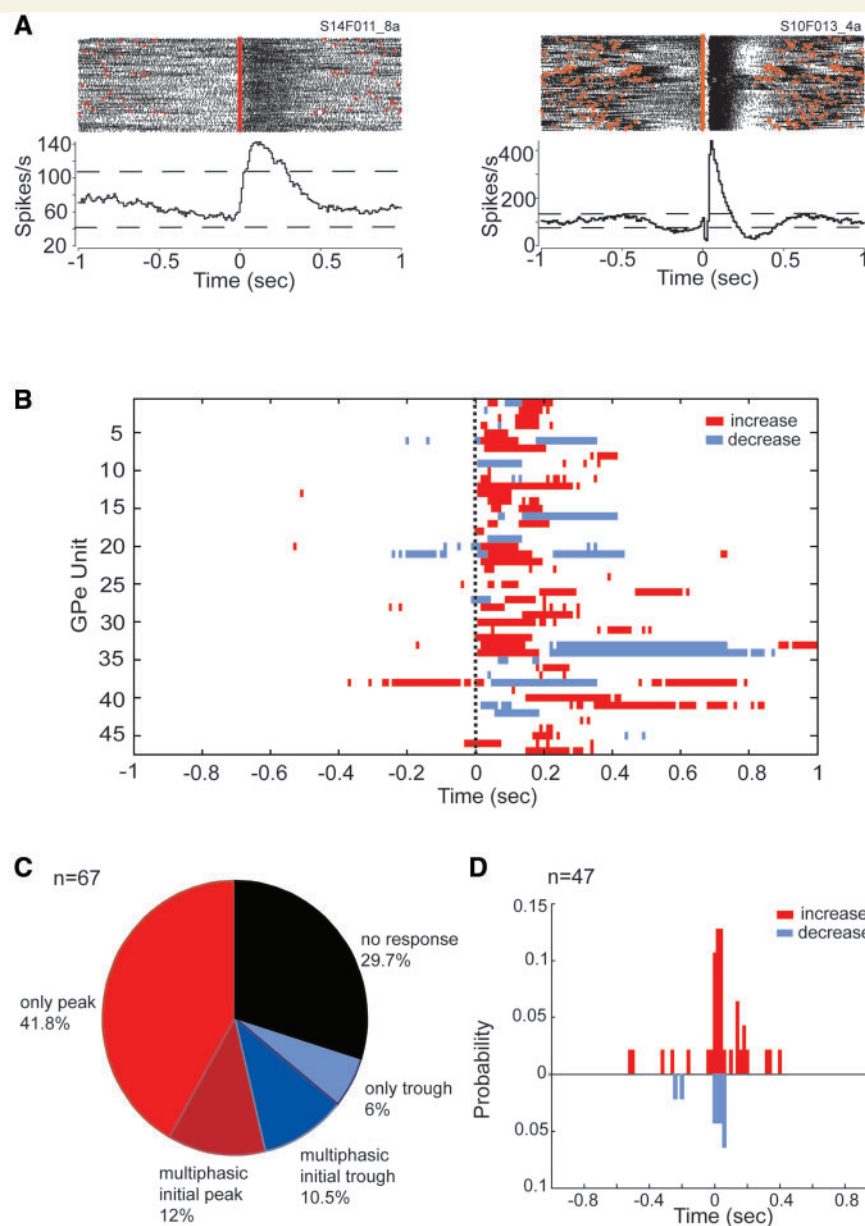
Figure 5 Neuronal firing changes surrounding motor tics in the GPe. (**A**) Peri-tic histograms and raster plots of two GPe neurons displaying the most common types of responses. Red triangles represent tic related LFP spikes and black dots represent spikes of the recorded unit. (**B**) Peri-tic histogram matrix of all responding GPe cells, only significant ($P < 0.01$) changes in rate are presented (red, increases; blue, decreases). (**C**) Distribution of peri-tic response types in the GPe. (**D**) Relative timing of the first significant change in the activity of responsive GPe cells aligned to LFP onset.

of their appearance and termination require further investigation, which was beyond the scope of the present study.

A dominant feature of the neurophysiological data set was the appearance, in each of the recording electrodes, of slow (several hundred ms) large (several millivolts) periodic LFP spikes that were closely correlated with the appearance of tics. Similar results of synchronous LFP activity in the striatum and cortex have been reported following GABA modulation in felines (McKenzie and Viik, 1975), rodents (McKenzie and Viik, 1975; Tarsy et al., 1978) and recently in primates (Darbin and Wichmann, 2008). This is the first study, however, to record at all the principal

nodes of the cortico-basal ganglia loop simultaneously, and to quantify the properties of these LFP spikes and their relations to behavioural tic events and single cell activity in different nuclei. Similar to the EMG data, the structure of each LFP event tended to be fixed in size and duration. In ours and in previous studies the LFP spikes were found to be concurrent with the onset of tics (Tarsy et al., 1978). Another study, however, has shown the existence of LFP spikes following striatal bicuculline micro-injection in the absence of obvious behavioural changes (Darbin and Wichmann, 2008), a phenomenon that we occasionally observed in our data as well. Taken together, this suggests that the LFP
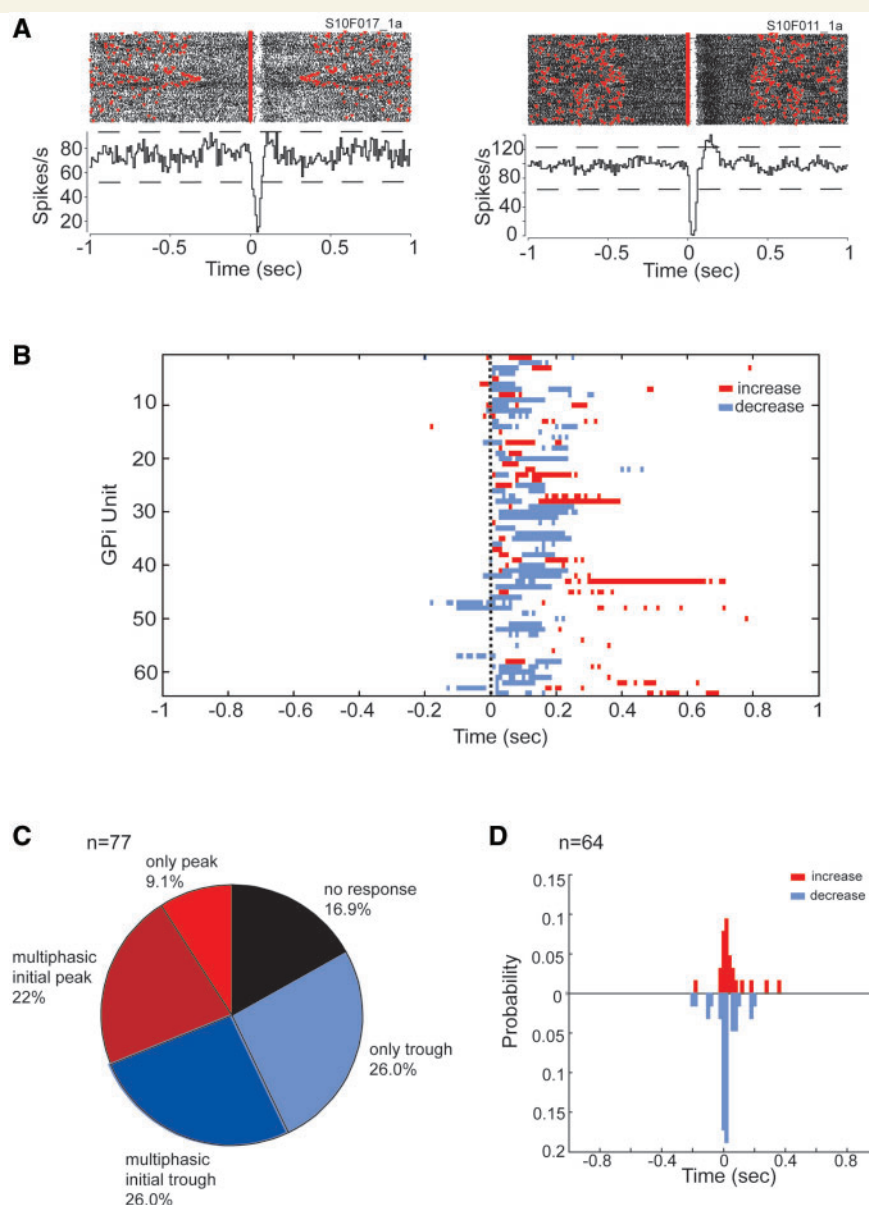
Figure 6 Neuronal firing changes surrounding motor tics in the GPi. (**A**) Peri-tic histograms and raster plots of two GPi neurons displaying the most common types of responses. Red triangles represent tic related LFP spikes and black dots represent spikes of the recorded unit. (**B**) Peri-tic histogram matrix of all responding GPi cells, only significant (*P*<0.01) changes in rate are presented (red, increases; blue, decreases). (**C**) Distribution of peri-tic response types in the GPi. (**D**) Relative timing of the first significant change in the activity of responsive GPi cells aligned to LFP onset.

spikes are not a result of a movement artifact caused by the motor tics, but rather represent a system-wide neurophysiological signal caused by the focal disinhibition in the striatum.

LFP signals are classically regarded as the sum of synaptic activity in a small area around the recording electrode, and are considered to represent the total synaptic input to a system (Mitzdorf, 1985; Logothetis, 2003). Accordingly, a large voltage deflection, as we saw in the LFP spikes, represents the synchronized activity of a large population of cells in the up-stream nuclei to the recording site. Thus, the LFP spikes may represent a time-locked recruitment and activation of large populations of neurons propagating along the cortico-basal ganglia axis. Support for this

hypothesis can be found in the large proportion of neurons showing major changes in their firing rate time-locked to the LFP spikes. LFP activity recorded in deep brain nuclei may result from passive conductance of the large LFP activity generated by the laminar organization of the cortex (Mitzdorf, 1985). Alternatively, deep brain LFP may result from localized LFP activity (Brown, 2003), which propagates via synaptic transmission along the cortico-basal ganglia loop. One way of differentiating between volume and synaptic transmission is the difference in propagation time, which is a few milliseconds. The LFP spikes we recorded had a long temporal structure (typically 200–350 ms total duration), making the identification of small
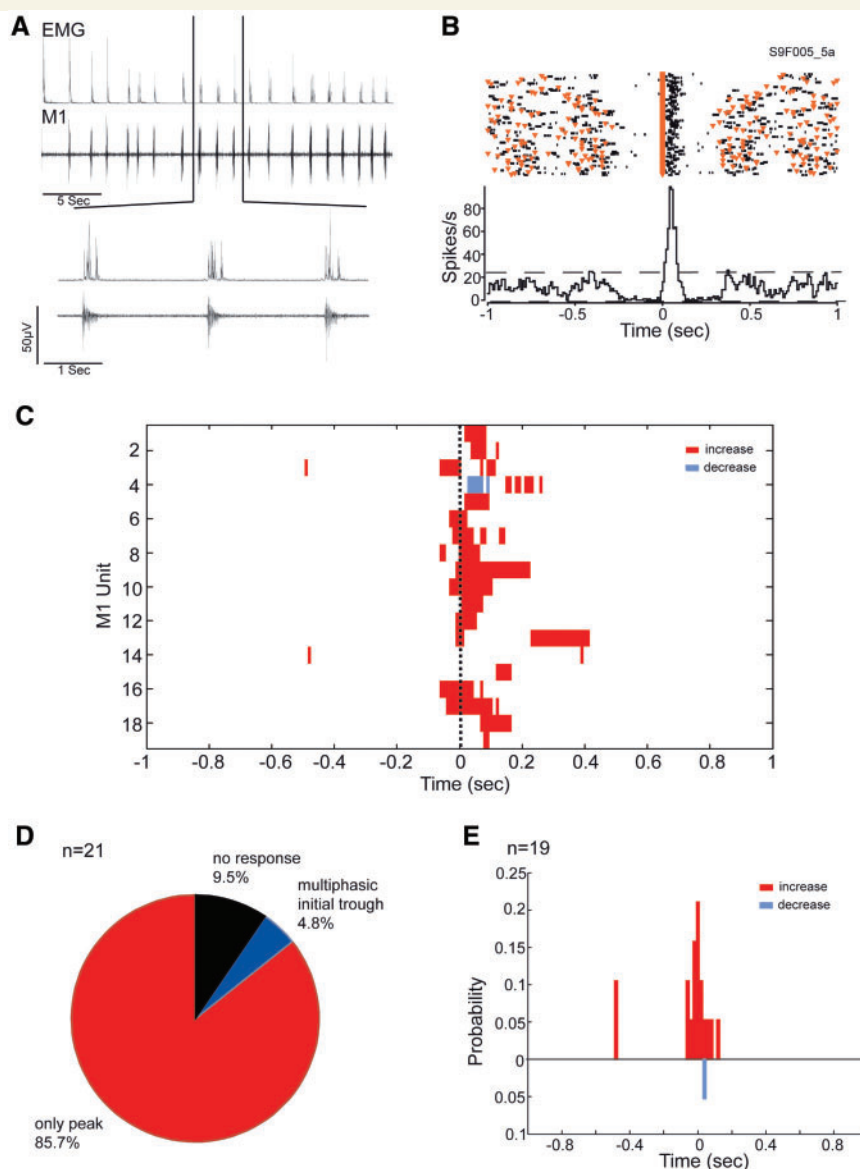
Figure 7 Neuronal firing changes surrounding motor tics in primary motor cortex (M1). (**A**) An example of a rectified EMG trace from the facial region (zygomaticus major) during tics (top trace) and a simultaneous recording from a single neuron in M1 (bottom trace). The magnified section shows the decrementing spike waveforms displayed by cortical neurons during the tic activity. (**B**) The peri-tic histogram and raster plot of a typical M1 cell aligned to LFP onset. Red triangles represent tic related LFP spikes and black dots represent spikes of the recorded unit. (**C**) Peri-tic histogram matrix of all responding M1 cells, only significant (P<0.01) changes in rate are presented (red, increases; blue, decreases). (**D**) Distribution of peri-tic response types in M1. (**E**) Relative timing of the first significant change in the activity of responsive M1 cells aligned to LFP onset.

timing differences between different brain structures problematic. This property, combined with the large variability seen in the timing of LFP-related neuronal activity, reflects the need for further research to shed light on the temporal dynamics of LFP propagation and its relation to single unit activity along the cortico-basal ganglia path.

The predominant response of the GPe neurons to striatal bicuculline injections was increased activity around the time of each tic. This increase in activity appears to be paradoxical in light of previous studies, which found that striatal projection neurons [medium spiny neurons (MSNs)] increase their firing rate

following local application of GABA antagonists (Bernardi et al., 1976; Nisenbaum and Berger, 1992; Kita, 1996; Darbin and Wichmann, 2008), which should, in theory, increase inhibition to the GPe via the indirect pathway. A new study by (Worbe et al., 2008) found that while MSNs close to the bicuculline injection site increase their firing rate, neurons located further away in the striatum decrease their firing rate. This suggests that local bicuculline injections may lead to a change in the dynamics of the entire striatal network, having complex effects on more distant neurons which are not directly influenced by the bicuculline. Only a small fraction (<2%) of striatal neurons were directly affected by the

bicuculline injections in our study, based on estimations of bicuculline spread (Yoshida *et al*., 1991) and total size of the putamen (Yin *et al*., 2009). Increased activity in the GPe, however, was evident throughout the nucleus (Supplementary Fig. 5), suggesting that the distant striatal network level effects were probably the key factor in modulating striatal output. Generalized effects outside the bicuculline-effected area in the striatum can be mediated by local axon collaterals of MSNs or by GABAergic interneurons which are known to exert powerful inhibition on striatal projection neurons and form wide spread networks throughout the nucleus (Koos and Tepper, 1999; Koos *et al*., 2004).

The most common effect of striatal bicuculline on GPi neurons was a phasic reduction in firing rate around each tic, leading in many cases to a complete cessation of firing. Overall inhibition of basal ganglia output following striatal administration of the GABA antagonist picrotoxin, has been previously reported; however, behavioural correlates were lacking due to the experimental preparation being anaesthetized (Obata and Yoshida, 1973). Similar tonic reductions in pallidal outflow in awake primates have been inferred from autoradiographic labeling following delivery of bicuculline to the striatum (Mitchell *et al*., 1985). There are several hypothetical mechanisms, which may explain the observed reductions in GPi activity. GPi neurons could be inhibited directly by activation of GPe neurons making GABAergic monosynaptic connections with GPi neurons (Sato *et al*., 2000; Kita, 2007), or indirectly due to a reduction of excitatory drive from the STN onto the GPi caused by over activity of inhibitory GPe neurons projecting to the STN (Nambu *et al*., 2002). Another potential mechanism could be hyperactivity within the direct pathway from the striatum to the GPi. In light of the increased activity in the GPe, however, suggesting a reduction in inhibitory outflow from the striatum during tic onset, it would appear likely that the reduced activity in the GPi is a consequence of the increased activity in the GPe.

The contribution of the basal ganglia to ongoing movement is widely accepted; however, the precise role of the basal ganglia output remains controversial. The GPe and GPi were shown to change their activity during volitional movement, displaying several types of phasic movement-related activity, with increases in firing rate being the more common response compared to decreases (DeLong, 1972; Turner and Anderson, 1997). The timing of globus pallidus activity relative to movement onset, however, is a matter of debate with some studies showing early globus pallidus activity (up to several hundred ms prior to movement onset) (Neafsey *et al*., 1978; Mitchell *et al*., 1987; Brotchie *et al*., 1991) and others showing that most globus pallidus movement-related activity is later than movement onset (DeLong *et al*., 1985; Turner and Anderson, 1997). It is not surprising that in our model we also found phasic changes of globus pallidus neuronal activity around tic-onset time; however, this activity was markedly different from the pattern of normal movement-related activity. While in the normal state globus pallidus neurons respond preferentially or exclusively to different movements, depending on various factors such as the movement location (body part being moved), direction, context, etc. (DeLong *et al*., 1985; Turner and Anderson, 2005), our results indicate that the majority of neurons

(70.3% in GPe, 83% in GPi) all respond to the same specific simple movement—the tic. In the normal state activity in the output structures of the basal ganglia shows a mixture of phasic increases and decreases. This pattern is believed to inhibit most of the thalamic targets of the basal ganglia while releasing a smaller population of the target neurons, leading to a focused selection of 'winning' actions accompanied by inhibition of competing actions (Mink, 1996; Albin and Mink, 2006). In contrast, we show that almost all GPi cells that respond to the tic show a reduction in firing rate, suggesting that once tic expression commences, GPi disinhibition of cortex is actually spatially distributed within the nuclei, rather than being focal in space. Therefore the transformation from the temporally specific but spatially distributed release of the action to the final activation which is specific in both space (focal tics) and time, most likely occurs downstream from the basal ganglia output.

Finally, the tics induced by striatal disinhibition bear a resemblance to motor tics in human pathologies that are known to be associated with basal ganglia dysfunction (detailed description in Supplementary Fig. 5). Thus, the neuronal changes observed during bicuculline induced tic formation may provide valuable insights into the underlying mechanism of human tic disorders as well as into basic information processing in the cortico-basal ganglia loop.

Supplementary material

Supplementary material is available at *Brain* online.

Acknowledgements

Funding

References

Albin RL, Mink JW. Recent advances in Tourette syndrome research. Trends Neurosci 2006; 29: 175–82.

Albin RL, Young AB, Penney JB. The functional anatomy of basal ganglia disorders. Trends Neurosci 1989; 12: 366–75.

Alexander GE, DeLong MR, Strick PL. Parallel organization of functionally segregated circuits linking basal ganglia and cortex. Annu Rev Neurosci 1986; 9: 357–81.

Beiser DG, Houk JC. Model of cortical-basal ganglionic processing: encoding the serial order of sensory events. J Neurophysiol 1998; 79: 3168–88.

Bernardi G, Marciani MG, Morucutti C, Giacomini P. The action of picrotoxin and bicuculline on rat caudate neurons inhibited by GABA. Brain Res 1976; 102: 379–84.

Bolam JP, Hanley JJ, Booth PA, Bevan MD. Synaptic organisation of the basal ganglia. J Anat 2000; 196 (Pt 4): 527–42.

Brotchie P, Iansek R, Horne MK. Motor function of the monkey globus pallidus. 1. Neuronal discharge and parameters of movement. Brain 1991; 114 (Pt 4): 1667–83.

Brown P. Oscillatory nature of human basal ganglia activity: relationship to the pathophysiology of Parkinson's disease. Mov Disord 2003; 18: 357–63.

Caviness JN, Brown P. Myoclonus: current concepts and recent advances. Lancet Neurol 2004; 3: 598–607.

Crossman AR, Mitchell IJ, Sambrook MA, Jackson A. Chorea and myoclonus in the monkey induced by gamma-aminobutyric acid antagonism in the lentiform complex. The site of drug action and a hypothesis for the neural mechanisms of chorea. Brain 1988; 111 (Pt 5): 1211–33.

Crossman AR, Sambrook MA, Jackson A. Experimental hemichorea/hemiballismus in the monkey. Studies on the intracerebral site of action in a drug-induced dyskinesia. Brain 1984; 107 (Pt 2): 579–96.

Darbin O, Wichmann T. Effects of striatal GABA-A receptor blockade on striatal and cortical activity in monkeys. J Neurophysiol 2008; 99: 1294–305.

de la Tourette G. Etude sur une Affection Nerveuse Caracterisee par de l'Incoordination Motrice Accompagnee d'Echolalie et de Coprolalie (jumping, lateh. myriachit). Arch Neurol 1885; 9: 19–42.

Defebvre L. Myoclonus and extrapyramidal diseases. Neurophysiol Clin 2006; 36: 319–25.

DeLong MR. Activity of basal ganglia neurons during movement. Brain Res 1972; 40: 127–35.

DeLong MR. Primate models of movement disorders of basal ganglia origin. Trends Neurosci 1990; 13: 281–5.

DeLong MR, Crutcher MD, Georgopoulos AP. Primate globus pallidus and subthalamic nucleus: functional organization. J Neurophysiol 1985; 53: 530–43.

DeLong MR, Wichmann T. Circuits and circuit disorders of the basal ganglia. Arch Neurol 2007; 64: 20–4.

Flaherty AW, Graybiel AM. Corticostriatal transformations in the primate somatosensory system. Projections from physiologically mapped body-part representations. J Neurophysiol 1991; 66: 1249–63.

Francois C, Grabli D, McCairn K, Jan C, Karachi C, Hirsch EC, et al. Behavioural disorders induced by external globus pallidus dysfunction in primates II. Anatomical study. Brain 2004; 127: 2055–70.

Gerfen CR, Wilson CJ. The basal ganglia. In: Swanson LW, Bjorklund A, Hokfelt T, editors. Handbook of chemical neuroanatomy. Part III. Elsevier Science: integrated systems of the CNS; 1996. p. 371.

Grabli D, McCairn K, Hirsch EC, Agid Y, Feger J, Francois C, et al. Behavioural disorders induced by external globus pallidus dysfunction in primates: I. Behavioural study. Brain 2004; 127: 2039–54.

Inase M, Sakai ST, Tanji J. Overlapping corticostriatal projections from the supplementary motor area and the primary motor cortex in the macaque monkey: an anterograde double labeling study. J Comp Neurol 1996; 373: 283–96.

Jankovic J, Ashizawa T. Tourettism associated with Huntington's disease. Mov Disord 1995; 10: 103–5.

Kalanithi PS, Zheng W, Kataoka Y, DiFiglia M, Grantz H, Saper CB, et al. Altered parvalbumin-positive neuron distribution in basal ganglia of individuals with Tourette syndrome. Proc Natl Acad Sci USA 2005; 102: 13307–12.

Kita H. Glutamatergic and GABAergic postsynaptic responses of striatal spiny neurons to intrastriatal and cortical stimulation recorded in slice preparations. Neuroscience 1996; 70: 925–40.

Kita H. Globus pallidus external segment. Prog Brain Res 2007; 160: 111–33.

Koos T, Tepper JM. Inhibitory control of neostriatal projection neurons by GABAergic interneurons. Nat Neurosci 1999; 2: 467–72.

Koos T, Tepper JM, Wilson CJ. Comparison of IPSCs evoked by spiny and fast-spiking neurons in the neostriatum. J Neurosci 2004; 24: 7916–22.

Kurlan R. Tourette's syndrome. In: Watts RL, William CK, editors. Movement disorders: neurologic principles & practice. McGraw-Hill Medical Publishing; 2004. p. 685–92.

Logothetis NK. The underpinnings of the BOLD functional magnetic resonance imaging signal. J Neurosci 2003; 23: 3963–71.

Marsden CD, Meldrum BS, Pycock C, Tarsy D. Focal myoclonus produced by injection of picrotoxin into the caudate nucleus of the rat. J Physiol 1975; 246: 96P.

Martin RF, Bowden DM. Primate brain maps. structure of the macaque brain. Elsevier Science; 2000.

Matsumura M, Sawaguchi T, Oishi T, Ueki K, Kubota K. Behavioral deficits induced by local injection of bicuculline and muscimol into the primate motor and premotor cortex. J Neurophysiol 1991; 65: 1542–53.

McKenzie GM, Viik K. Chemically induced chorieform activity: antagonism by GABA and EEG patterns. Exp Neurol 1975; 46: 229–43.

Mink JW. The basal ganglia: focused selection and inhibition of competing motor programs. Prog Neurobiol 1996; 50: 381–425.

Mink JW. Basal ganglia dysfunction in Tourette's syndrome: a new hypothesis. Pediatr Neurol 2001; 25: 190–8.

Mink JW. The basal ganglia and involuntary movements: impaired inhibition of competing motor patterns. Arch Neurol 2003; 60: 1365–8.

Mitchell IJ, Jackson A, Sambrook MA, Crossman AR. Common neural mechanisms in experimental chorea and hemiballismus in the monkey. Evidence from 2-deoxyglucose autoradiography. Brain Res 1985; 339: 346–50.

Mitchell SJ, Richardson RT, Baker FH, DeLong MR. The primate globus pallidus: neuronal activity related to direction of movement. Exp Brain Res 1987; 68: 491–505.

Mitzdorf U. Current source-density method and application in cat cerebral cortex: investigation of evoked potentials and EEG phenomena. Physiol Rev 1985; 65: 37–100.

Miyachi S, Lu X, Imanishi M, Sawada K, Nambu A, Takada M. Somatotopically arranged inputs from putamen and subthalamic nucleus to primary motor cortex. Neurosci Res 2006; 56: 300–8.

Nambu A, Tokuno H, Takada M. Functional significance of the cortico-subthalamo-pallidal 'hyperdirect' pathway. Neurosci Res 2002; 43: 111–7.

Neafsey EJ, Hull CD, Buchwald NA. Preparation for movement in the cat. II. Unit activity in the basal ganglia and thalamus. Electroencephalogr Clin Neurophysiol 1978; 44: 714–23.

Nisenbaum ES, Berger TW. Functionally distinct subpopulations of striatal neurons are differentially regulated by GABAergic and dopaminergic inputs—I. In vivo analysis. Neuroscience 1992; 48: 561–78.

Obata K, Yoshida M. Caudate-evoked inhibition and actions of GABA and other substances on cat pallidal neurons. Brain Res 1973; 64: 455–9.

Obeso JA, Rothwell JC, Lang AE, Marsden CD. Myoclonic dystonia. Neurology 1983; 33: 825–30.

Parent A, Hazrati LN. Functional anatomy of the basal ganglia. I. The cortico-basal ganglia-thalamo-cortical loop. Brain Res Brain Res Rev 1995; 20: 91–127.

Percheron G, Filion M. Parallel processing in the basal ganglia: up to a point. Trends Neurosci 1991; 14: 55–9.

Redgrave P, Prescott TJ, Gurney K. The basal ganglia: a vertebrate solution to the selection problem? Neuroscience 1999; 89: 1009–23.

Sato F, Lavallee P, Levesque M, Parent A. Single-axon tracing study of neurons of the external segment of the globus pallidus in primate. J Comp Neurol 2000; 417: 17–31.

Singer HS, Minzer K. Neurobiology of Tourette's syndrome: concepts of neuroanatomic localization and neurochemical abnormalities. Brain Dev 2003; 25 (Suppl 1): S70–84.

Szabo J, Cowan WM. A stereotaxic atlas of the brain of the cynomolgus monkey (Macaca fascicularis). J Comp Neurol 1984; 222: 265–300.

Tarsy D, Pycock CJ, Meldrum BS, Marsden CD. Focal contralateral myoclonus produced by inhibition of GABA action in the caudate nucleus of rats. Brain 1978; 101: 143–62.

Tepper JM, Koos T, Wilson CJ. GABAergic microcircuits in the neostriatum. Trends Neurosci 2004; 27: 662–9.

The Tourette Syndrome Classification Study Group. ''Definitions and classification of tic disorders. The Tourette Syndrome Classification Study Group''.1993; 10: 1013.

Turner RS, Anderson ME. Pallidal discharge related to the kinematics of reaching movements in two dimensions. J Neurophysiol 1997; 77: 1051–74.

Turner RS, Anderson ME. Context-dependent modulation of movement-related discharge in the primate globus pallidus. J Neurosci 2005; 25: 2965–76.

Vercueil L. Myoclonus and movement disorders. Neurophysiol Clin 2006; 36: 327–31.

Worbe Y, Baup N, Grabli D, Chaigneau M, Mounayar S, McCairn K, et al., Behavioral and movement disorders induced by local inhibitory dysfunction in primate striatum. Cereb Cortex 2008 (Epub ahead of print).

Yin D, Valles FE, Fiandaca MS, Forsayeth J, Larson P, Starr P, et al. Striatal volume differences between non-human and human primates. J Neurosci Methods 2009; 176: 200–5.

Yoshida M, Nagatsuka Y, Muramatsu S, Niijima K. Differential roles of the caudate nucleus and putamen in motor behavior of the cat as investigated by local injection of GABA antagonists. Neurosci Res 1991; 10: 34–51.

Zohar AH, Pauls DL, Ratzoni G, Apter A, Dycian A, Binder M, et al. Obsessive–compulsive disorder with and without tics in an epidemiological sample of adolescents. Am J Psychiatry 1997; 154: 274–6.